frontiers | Frontiers in Materials

TYPE Original Research
PUBLISHED 31 August 2023
DOI 10.3389/fmats.2023.1239692

OPEN ACCESS

EDITED BY
Rafael Comesaña,
University of Vigo, Spain

REVIEWED BY
Deepak M. Kalaskar,
University College London,
United Kingdom
Mozhgan Keshavarz,
University of California, Irvine,
United States

*CORRESPONDENCE
Hani A. Awad,
hani_awad@urmc.rochester.edu

RECEIVED 13 June 2023
ACCEPTED 14 August 2023
PUBLISHED 31 August 2023

CITATION
Yan M and Awad HA (2023), Optimizing rheological properties for printability: low-temperature extrusion 3D printing of hydroxyapatite-polycaprolactone mixture inks for bone tissue engineering. *Front. Mater.* 10:1239692. doi: 10.3389/fmats.2023.1239692

Optimizing rheological properties for printability: low-temperature extrusion 3D printing of hydroxyapatite-polycaprolactone mixture inks for bone tissue engineering

Ming Yan[1,2] and Hani A. Awad[1,2,3]*

[1]The Center for Musculoskeletal Research, University of Rochester, Rochester, NY, United States, [2]Department of Biomedical Engineering, University of Rochester, Rochester, NY, United States, [3]Department of Orthopaedics, University of Rochester, Rochester, NY, United States

Introduction: Low-temperature extrusion three-dimensional printing (LTE-3DP) using viscous ceramic-polymer inks has shown promise for bone tissue engineering. This process involves formulating a flowable ink by combining ceramic powders and other components with organic or inorganic polymer solutions, which can then be extruded through a 3D printer nozzle. LTE-3DP allows the incorporation of high fractions of bioactive ceramics and thermally labile additives such as drugs, proteins, and biomolecules into the inks to promote osteogenesis and bone regeneration. The rheology of the ink, influenced by various variables, significantly impacts the printability and form fidelity of the resulting scaffolds. These variables include the composition of the polymer solution and the size and weight ratio of ceramic microparticles. In this study, we posited that the printability of hydroxyapatite (HA) and polycaprolactone (PCL) mixture inks could be optimized by tailoring their rheological properties.

Methods: We conducted a systematic investigation, varying the PCL weight percentage and HA:PCL weight ratio, to examine the effects of the ink's composition on its viscosity and storage modulus, as well as its printability and the mechanical properties of 3D printed HA:PCL scaffolds.

Results: We demonstrated that HA:PCL inks exhibit predictable non-Newtonian fluid behavior at higher fractions of HA, displaying significant shear thinning at elevated shear rates, which can facilitate extrusion through a 3D printing nozzle. We identified printable ink compositions based on filament continuity and scaffold form fidelity criteria. Moreover, we performed computational simulations to analyze the ink flow through an extrusion nozzle. These simulations utilized the Herschel-Bulkley-Papanastasiou constitutive model, considering the rheological properties obtained from experimental measurements. By combining experimental measurements and computational simulations, we formulated a non-dimensional Printability number that predicts whether an ink is printable based on the ink's rheological parameters and printer-specific factors. Furthermore, we evaluated the compressive properties of printed HA:PCL scaffolds and characterized the effects of PCL% and HA:PCL ratio on the hyperelasticity observed in response to compressive deformations.

Discussion: This hybrid approach using experimental rheology and FE simulations provides a framework to define the printability of ceramic-polymer ink formulations, which could help streamline the 3D printing of novel inks for bone tissue engineering.

KEYWORDS

bone, extrusion 3D printing, hydroxyapatite, polycaprolactone, printability, rheological properties, hyperelasticity

1 Introduction

Massive bone loss resulting from infections, tumor resection, and traumatic fractures poses significant challenges in orthopaedics (Miranda and Moon, 2007; Campana et al., 2014; Hak et al., 2014). Although processed bone allografts have been traditionally employed for bone reconstruction, they exhibit drawbacks such as foreign body responses, disease transmission risks, and limited remodeling capacity, which could lead to nonunion and microfracture accumulation (Athanasiou et al., 2009; Hak et al., 2014). Therefore, the development of alternative bone graft substitutes has become crucial. An ideal substitute should fulfill four essential criteria: biocompatibility, osteoconductivity, osteoinductivity, and adequate mechanical properties. Furthermore, the substitute should facilitate easy and rapid installation by surgical teams while accommodating diverse geometrical constraints (Dorozhkin, 2010; Jakus et al., 2016b; Trombetta et al., 2017). Unfortunately, most commercially available bone void fillers lack customization capabilities due to their fixed geometries produced through standard fabrication techniques (Wang and Yeung, 2017). However, the emergence of three-dimensional (3D) printing technology offers a promising solution, enabling the creation of patient-tailored scaffolds for bone reconstruction in orthopedic and oral maxillofacial surgeries (Seitz et al., 2005; Travitzky et al., 2014; Trombetta et al., 2017; Zhang et al., 2019).

Ceramics, such as calcium phosphates (CaP), hydroxyapatite (HA), and Bioactive glass, are widely used for bone scaffolds and 3D printing due to their biocompatibility, intrinsic osteoinductive properties, high compressive strength, and slow biodegradability (Leukers et al., 2005; Seitz et al., 2005; Chen et al., 2015). However, these materials have certain drawbacks. Traditional 3D-printed ceramic scaffolds often require sintering at high temperatures yielding rigid scaffolds that exhibit brittle mechanical characteristics that make their surgical implementation challenging (Bohner, 2010; Zhang et al., 2014). Moreover, the high sintering temperature is incompatible with directly incorporating heat labile additives such as antibiotics, growth factors, and other molecules (Mouriño and Boccaccini, 2010). Alternatively, ceramic-polymer composite scaffolds can be produced at room temperature by extrusion–based 3D printing, effectively overcoming these drawbacks.

Ceramic-polymer composites offer tunable biological and mechanical properties compared to pure ceramics or polymers. In ceramic-polymer materials, ceramic powders such as HA, CaP, or Bioglass are dispersed in a polymer matrix such as poly (lactic-co-glycolic) acid (PLGA) or polycaprolactone (PCL). These composite materials can be 3D printed using extrusion through a nozzle as a hot melt or a viscous organic solution (Shor et al., 2007; Jakus et al., 2016a). Hot melt or thermal printing is a traditional printing method with several disadvantages. Firstly, the amount of ceramic powder that can be added is limited to avoid nozzle clogging and is typically less than 5% of the polymer mass. Secondly, while the temperature required for polymer melting is considerably lower (between 60°C and 130°C) compared to the >1,000°C needed for ceramic sintering, it still hinders the direct incorporation of biological molecules or factors (Dwivedi et al., 2020). Alternatively, ceramics such as CaP can be dispersed at high concentrations in polymers dissolved in volatile organic solvents to form a viscous and non-newtonian solution known as ink. The shear thinning properties of the ink facilitate its extrusion through the printing nozzle, while its viscosity allows it to maintain structure and shape fidelity after printing until the volatile solvent evaporates, solidifying the ceramic-polymer scaffold (Gillispie et al., 2020; Naghieh and Chen, 2021; Tarassoli et al., 2021). For example, Jakus et al. (2016a) generated hyperelastic bone scaffolds composed of HA and PCL or PLGA (90:10 wt%). These scaffolds could be rapidly 3D printed at room temperature and demonstrated robust osteoinductive properties in animal models (Jakus et al., 2016a; Huang et al., 2019).

While these studies and others demonstrate the feasibility of low-temperature extrusion three-dimensional printing (LTE-3DP) of viscous ceramic-polymer inks for bone tissue engineering, optimizing the LTE-3DP of a particular ink depends on several variables. These variables include type, molecular weight, concentration of polymer, choice of solvent, presence of additives such as plasticizer and surfactant, and the type, size, ratio, and doping of the ceramic nano- or micro-particles. In particular, these variables influence the viscosity and flowability of the ink and the shape fidelity and mechanical properties of the 3D-printed scaffolds. Although the significance of these variables has been acknowledged in the literature (Gillispie et al., 2020; Naghieh and Chen, 2021), a limited number of studies have methodically investigated the impact of these ink variables on printability. In this study, we hypothesized that the printability of polymer-ceramic materials could be enhanced by optimizing their rheological properties. To investigate this hypothesis, we focused on a standard ink consisting of polycaprolactone (PCL) and hydroxyapatite (HA) 3D printing. By systematically varying the PCL concentrations and HA:PCL ratio, we evaluated their effects on the bulk rheology of the ink to model the non-Newtonian flow through the 3D printing nozzle. Furthermore, we determined the critical parameters that govern the printability of HA:PCL scaffolds and their mechanical properties. The combination of experimental rheology and numerical simulations in this hybrid approach establishes a framework for streamlining the design of inks for extrusion 3D printing of ceramic-polymer scaffolds for bone tissue engineering.

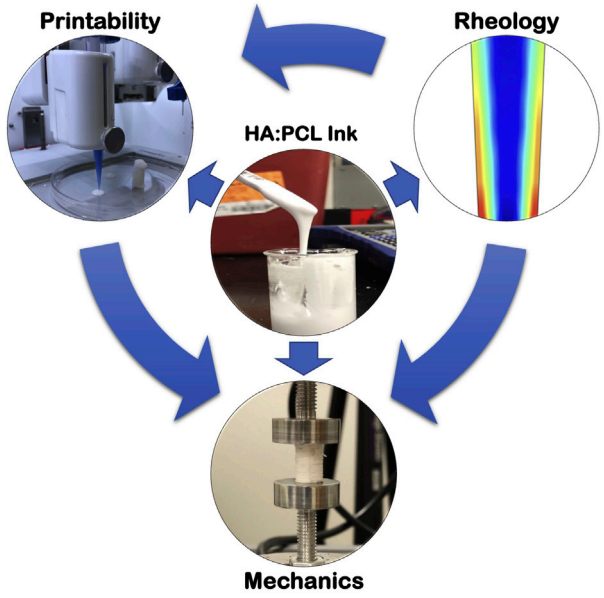

FIGURE 1
Extrusion 3D-printing of tunable HA:PCL porous scaffolds. Polycaprolactone (PCL) is dissolved in Dichloromethane (DCM) with plasticizers (Dibutyl phthalate (DBP) and 2-Butanone (2-Bu) at concentrations from 15% to 30% w/v. The solution is mixed with HA microparticles at weight ratios (HA:PCL) ranging from 1:1–9:1 to create viscous mixtures, which can be printed using an extrusion-based BioX™ 3D printer. The HA:PCL ink formulation, encompassing different PCL% and HA:PCL weight ratios, dictates its rheological behavior, which subsequently affects the printability and the mechanical properties of the resulting scaffolds.

2 Materials and methods

This paper describes the preparation of polymer-ceramic inks and investigates the effects of various parameters on the rheological properties, printability, and mechanical properties of the printed scaffolds (Figure 1). These parameters included organic solvent composition, different weight concentrations of PCL (15%–30%), and different ceramic-to-polymer weight ratios (1:1–9:1). By computationally simulating the flow of ink in a 3D printing nozzle, we explored the effect of experimentally determined rheological properties on the printability of ink. We then cross-referenced the computational results with actual printing results to identify a range of printable ink formulations. Subsequently, we performed mechanical tests to assess the effect of different ink compositions on the mechanical properties of the printed scaffolds.

2.1 Preparation of 3D printing inks

A ternary solvent was prepared by mixing Dichloromethane (DCM, CH_2Cl_2, Sigma, Cat# 270997) with the surfactant 2-butoxyethanol ($BuOC_2H_4OH$, Sigma, Cat# 111-76-2), and the plasticizer dibutyl phthalate [DBP, C_6H_4 $(CO_2C_4H_9)_2$, Sigma, Cat# 524980] in a volumetric ratio of 5:3:1. Polycaprolactone (PCL, Mn = 80,000, Sigma, Cat# 440744) was dissolved into the three-component or two-component solvents at concentrations of 15%, 20%, 25%, and 30 to create PCL solutions. Hydroxyapatite powder (HA, Sigma, Cat# 289396) was sieved through a 30-micron mesh and combined with different PCL solutions at weight ratios (HA:PCL) ranging from 1:1 to 9:1 to generate a library of ink formulations.

2.2 Rheological characterization of inks

Rheological testing was performed using an Anton-Paar MCR 302 rheometer (Anton Paar United States Inc., Ashland, VA) equipped with a parallel-plate geometry (PP25/TG parallel-plate 24.982 mm diameter and 0.5 mm gap) for all the ink formulas, including all concentrations of pure PCL solutions. For each test, 5 mL ink was loaded, and the measuring plate was lowered into position. To prevent solvent evaporation, mineral oil was applied to the edges of the sample under the plate. An oscillatory shear rate sweep was performed from 0.1 to 10 s^{-1}, and the viscosity data was collected by the rheometer. Subsequently, the plate was cleaned, and another 5 mL of the same ink was loaded. An oscillatory time sweep was performed for 6,000 s, during which the rheometer collected data on the storage modulus. This was subsequently repeated for all ink formulations.

2.3 Finite element simulations

Finite element fluid flow simulations were conducted in COMSOL Multiphysics® (Palo Alto, CA). The simulation 3D printing nozzle was modeled using a standard 27G conical nozzle (200 μm orifice). A mesh composed of free tetrahedral elements was employed. The boundary conditions for the inlet pressure ranged from 0.5 to 7 bar, which corresponds to the inlet pressure range of the BioX 3D printer. The outlet pressure was set to atmospheric conditions. The flow behavior of the ink formulations was simulated using an incompressible, non-Newtonian fluid model known as the Herschel-Bulkley-Papanastasiou model, which was initially proposed by Papanastasiou in 1987 (Frigaard and Nouar, 2005; Wang et al., 2023). The HBP model can be written as,

$$\eta_{eff} = K\dot{\gamma}^{(n-1)} + 2\dot{\gamma}^{\left(1-e^{-2m\dot{\gamma}}\right)} \tag{1}$$

in which η_{eff} is the effective viscosity, $\dot{\gamma}$ represents shear rate, K and m are model coefficients, and n represents the flow behavior index.

The constant coefficient m can be obtained by solving

$$m = \lim_{\dot{\gamma}\to 0} \frac{1}{2\dot{\gamma}} \left(1 - e^{-2m\dot{\gamma}}\right) \tag{2}$$

Alternatively, the Herschel-Bulkley model (von Boetticher et al., 2016) can also be expressed as:

$$\tau = \tau_y + K\dot{\gamma}^n \tag{3}$$

In Eq. 3, τ represents the shear stress of the fluid, and τ_y is the yield shear stress of the fluid. This equation describes the relationship between the constants n (the flow behavior index) and K (the consistency coefficient). Eq. 3 can be rewritten as Eq. 4 to estimate constants n and K by fitting the experimentally determined rheological shear stress and shear rate data.

$$\log_{10}\left(\tau - \tau_y\right) = \log_{10}K + n\log_{10}\dot{\gamma} \tag{4}$$

For all ink formulations, simulations were conducted to obtain the spatial distributions of the shear stress, shear rate, and dynamic viscosity within the nozzle. All simulations and convergence criteria were verified to be grid-independent, ensuring that all discretization errors converged to zero.

2.4 3D printing

A BioX™ 3D printer with a 27G conical nozzle (200 μm) was used to print the various ink formulas, ranging from 15% to 30%, with mixtures of HA:PCL ratios ranging from 1:1 to 9:1 into standard porous cylinders (2 mm diameter, 10 mm height) featuring a rectangular lattice structure and a fill-up ratio of 90%. The printing process commenced at ambient temperature with an inlet pressure of 50 kPa, gradually increasing until the ink could be extruded continuously. The inlet pressure values were recorded for each ink formula, and in general printable ink formulas were successfully printed at 200 kPa. A consistent print speed of 8 mm/s was maintained for all ink formulas, and the nozzle tip to print platform distance was fixed at 150 μm. The resulting structures were assessed qualitatively based on filament integrity and self-supportiveness, which dictate form fidelity. All the data was compiled and organized into a printability matrix. Following printing, the structures were left to dry in a chemical hood for 2 h.

2.5 Mechanical testing

Compression testing of cylindrical disks (Diameter = 8 mm, Height = 16 mm), 3D printed with 90% fill ratio, was conducted on an Instron 8841 DynaMight™ Axial Testing System (Instron Corp.; Canton, MA, United States) with a 50 N load cell. The disks were compressed at a constant displacement rate of 2 mm/min until densification (near vertical stress v.s. strain curve). Six specimens were tested for each of the selected ink formulations.

Since the materials exhibited a hyperelastic behavior, the stress-strain curves were fitted to the Mooney-Rivlin hyperelastic material with five parameters (Umale et al., 2013; Kumar and Rao, 2016; Shi-Ju et al., 2020). Generally, the material model is defined by a strain energy density function W, which can be described as a function of the principal stretch ratios $\lambda_1, \lambda_2,$ and λ_3.

$$W = f(\lambda_1, \lambda_2, \lambda_3) \tag{5}$$

The principal stretch ratios λ, are defined as the ratios of the length L of a deformed sample to the thickness L_0 in each axis,

$$\lambda = \frac{L}{L_0} \tag{6}$$

All inks were considered incompressible, which implied that $\lambda_1\lambda_2\lambda_3 = 0$.

In each axis, the principal Cauchy stresses, σ_i, for an incompressible material, defined per unit cross-sectional area normal to the axis in the deformed configuration, are related to stretches through W, as expressed in Eq. 7.

$$\sigma_i = \lambda_i\frac{\partial W}{\partial \lambda_i} - p \tag{7}$$

where p is an undetermined hydrostatic pressure introduced because of the incompressibility constraint, which can be determined from the boundary conditions.

The strain energy density function and Cauchy stress of inks according to the five-parameter Mooney-Rivlin model can be expressed as:

$$W = c_1(I_1 - 3) + c_2(I_2 - 3) + c_3(I_1 - 3)(I_2 - 3) + c_4(I_1 - 3)^2 + c_5(I_2 - 3)^2 \tag{8}$$

$$\sigma = 2\left(\lambda^2 - \frac{1}{\lambda}\right)\left[c_1 + \frac{c_2}{\lambda} + 3c_3\left(\frac{1}{\lambda^2} - 1\right)(1 - \lambda) + 2c_4\left(\lambda^2 + \frac{2}{\lambda} - 3\right) + \frac{2c_5}{\lambda}\left(\frac{1}{\lambda^2} + 2\lambda - 3\right)\right] \tag{9}$$

In the above expressions, I_1 and I_2 are the first and second invariants of the deformation tensor, and c_i are material parameters.

$$I_1 = \sum_{i=1}^{3}(\lambda_i)^2 \tag{10}$$

$$I_2 = (\lambda_1)^2(\lambda_2)^2 + (\lambda_2)^2(\lambda_3)^2 + (\lambda_3)^2(\lambda_1)^2 \tag{11}$$

The "fit" function in the curve fitting toolbox of MATLAB® (MATLAB and Statistics Toolbox Release 2019a, The MathWorks, Inc.) was used to fit the model to the experimentally measured stresses. The initial guess for the material model parameters was randomly chosen, and the Trust- Region-Reflective algorithm was used for the fitting procedure. The goodness of fit was analyzed by the sum of squares due to error (SSE), R-square, Adjusted R^2, and Root mean squared error (RMSE).

2.6 Statistics

GraphPad Prism 9 (Version 9.5.0) was used to perform the statistics. Where appropriate, data were analyzed using analysis of variance (ANOVA) with Bonferroni corrections for multiple comparisons as indicated within the Results section. Data from each metric was confirmed to satisfy assumptions of a Gaussian distribution based on the D'Agostino-Pearson normality test, or a non-parametric alternative was used where appropriate. Differences were considered significant for $p < 0.05$.

3 Results

3.1 Rheological characterization of HA:PCL mixture inks

Rheological testing of inks formulated by dissolving PCL in ternary solvents demonstrated proportional increases in the dynamic viscosity of the ink with increased PCL%. However, except for the 30% PCL, the dynamic viscosity did not vary with increased shear rates, indicating that the dilute pure PCL inks at concentrations <30% behave as Newtonian fluids (Figure 2A). The storage modulus of the pure PCL inks does not vary significantly with increasing PCL% (Figure 2B), suggesting that the increase in viscosity does not alter the fluid behavior of the ink.

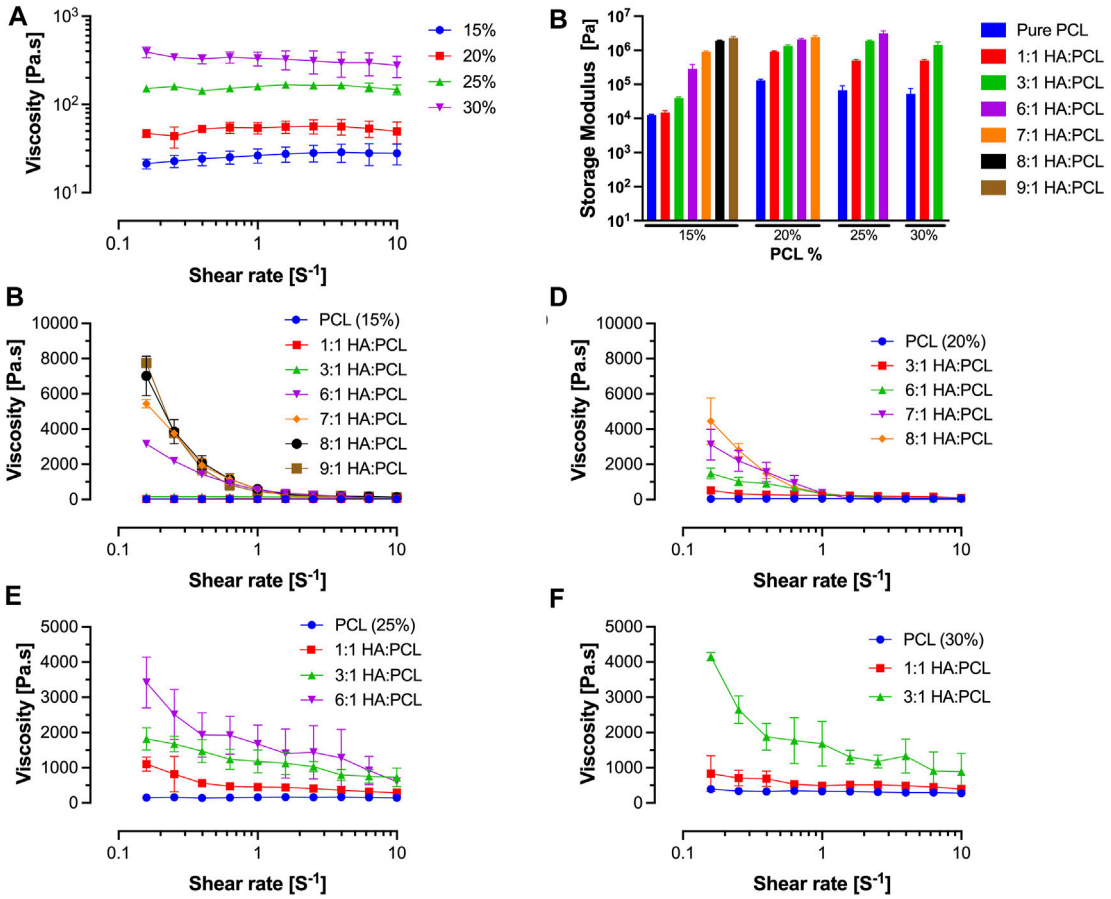

FIGURE 2
Rheological evaluation of HA:PCL mixture inks. **(A)** Flow (shear rate) sweep of pure polycaprolactone (PCL) dissolved in a ternary solvent at 15% to 30% w/v concentrations. Pure PCL-only inks do not exhibit signficant shear thinning. **(B)** Storage modulus determined from oscillatory time sweep experiments of HA:PCL inks. The storage modulus of the pure PCL inks does not vary significantly with increasing PCL%; however, it increases with increasing HA:PCL ratio, which suggests that these viscous inks possess solid-like properties. **(C)** Flow (shear rate) sweep of 15% PCL in a ternary solution mixed with HA microparticles at weight ratios ranging from 1:1 to 9:1 (HA:PCL). **(D)** Flow (shear rate) sweep of 20% PCL in a ternary solution mixed with HA microparticles at weight ratios ranging from 1:1 to 8:1 (HA:PCL). **(E)** Flow (shear rate) sweep of 25% PCL in a ternary solution mixed with HA microparticles at weight ratios ranging from 1:1 to 6:1 (HA:PCL). **(F)** Flow (shear rate) sweep of 30% PCL in a ternary solution mixed with HA microparticles at weight ratios ranging from 1:1 to 3:1 (HA:PCL). Data represent the average and standard deviation of six samples (n = 3).

Furthermore, increasing the ratio of HA:PCL leads to an increase in the dynamic viscosity of the inks at low shear rates, regardless of the PCL% (Figures 2C–F). With the increased ratio of HA:PCL, the inks exhibit shear thinning behavior, as evident by the decrease in the dynamic viscosity of the ink during the shear rate sweeps. The increased PCL% and HA:PCL ratio result in highly viscous inks. However, the demonstrable shear thinning at high shear rates corresponding to flow rates experienced during the extrusion printing process suggests that these viscous inks can be printable. On the other hand, increasing the ratio of HA:PCL significantly increases the storage modulus of the inks (Figure 2B). Bioinks with high storage modulus and solid-like properties are less prone to shape distortion caused by gravitational forces or other external influences. This is particularly critical when the printed structures require time to solidify as the solvent evaporates. Therefore, the proportional increases in the storage modulus with increased HA:PCL ratios could improve shape fidelity, ensuring that the printed scaffold closely matches the digital design.

3.2 Qualitative evaluation of printability

To qualitatively evaluate their printability, several ink formulations (PCL% from 15% to 30% and HA:PCL ratio from 1:1 to 9:1) were printed through conical bioprinting nozzles with 200 µm tip opening using a BioX™ extrusion 3D printer. A printability matrix was constructed by qualitative assessment of the integrity of the filaments as they were extruded and visual evidence of self-supporting properties and shape fidelity of the final printed scaffolds (Figure 3). Pure PCL inks or inks with a 1:1 HA:PCL ratio were too soft and exhibited poor shape fidelity, regardless of the PCL%. For the 15% PCL inks, shape fidelity was achieved at HA:PCL ratios greater than 8:1. However, with increasing PCL%, the maximum HA:PCL ratio permissive of printability decreased. For example, while 6:1 HA:PCL (25%) inks were printable, increasing the HA:PCL ratio to 7:1 resulted in discontinuities in the extruded filaments, and increasing it further to 8:1 resulted in nozzle clogging, rendering these inks unprintable.

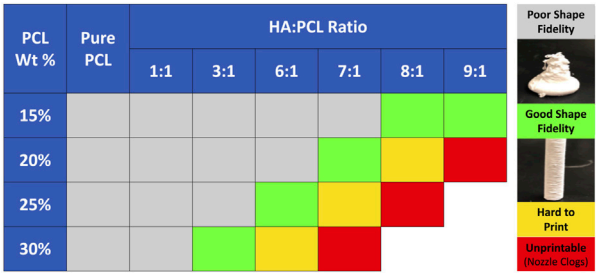

FIGURE 3
Printability matrix for HA:PCL mixture inks. PCL was dissolved in ternary solvents at 15%–30% w/v concentrations. Final inks were prepared by mixing HA with the PCL solution at HA:PCL weight ratios ranging from 1:1 to 9:1. All the bio-ink formulas were printed through a 200 μm conical nozzle using an extrusion-based BioX™ 3D bioprinter. The scaffolds were designed as 8 mm diameter x 16 mm height cylinders with a 90% fill ratio. Printable formulations were defined as those that allow 3D printing without filament discontinuities or nozzle clogging and without collapsing after printing.

3.3 Printability prediction based on FE simulations of ink flow within the bioprinter nozzle

An incompressible, non-Newtonian fluid [Herschel-Bulkley-Papanastasiou (HBP)] model was used to simulate the flow of all the ink formulas. The flow behavior index (n) and the consistency coefficient (K) were empirically determined by fitting the rheology data to Eq. 4 (Table 1). As the PCL% and HA:PCL ratio increased, K trended upwards, indicating higher resistance to flow under shear stress (Figure 4A). Although the impact of PCL% on the flow index (n) is relatively minor, for a specific PCL% and HA:PCL ratios <6:1, n decreases with increased HA:PCL ratio. However, as the ink suspension becomes more viscous with higher HA:PCL ratios (>6:1), an upward trend in the value of n is observed with increased HA:PCL ratios. In all cases, the value of n remains below 1, which aligns with the pseudoplastic shear thinning behavior observed in HA:PCL suspension inks (Figure 4B).

A conical 200 μm printing nozzle was used for the finite element simulation. Each ink formulation was simulated with varying extrusion pressures (boundary conditions) ranging from 100 kPa to 700 kPa (Figure 5A). Using the example of a 20% PCL with an 8:1 HA:PCL ratio, the shear rate is highest at the nozzle walls, while the visosity profiles at different extrusion pressures show parabolic distributions with maxima in the center of the nozzle and minima at the walls (Figure 5B). For a given HA:PCL ratio, increasing the extrusion pressure from 100 kPa to 200 kPa decreases the maximum viscosity. Figure 5C shows the computed dynamic viscosity profiles for several HA-PCL ratios at the ejection boundary for extrusion pressures of 100 kPa and 200 kPa, respectively. For a given extrusion pressure (200 kPa), the simulation shows that increasing the HA:PCL ratio increases the viscosity, which is consistent with experimental rheology data.

To establish the optimal range of maximum (or average) dynamic viscosity within the nozzle for enhanced printability, a surface plot depicting the maximum viscosity at the ejection orifice of the nozzle was generated for all simulated inks at an extrusion pressure of 200 kPa (Figure 6A). The printable formulations obtained through experimental testing at this pressure exhibited viscosities clustered closely within a defined range, represented by circles on the surface plot. To precisely define this range, a bar plot illustrating the simulated maximum viscosity at the nozzle's orifice was created for all inks tested in the experiments (Figure 6B). For printable inks (Figure 3), we have empirically determined that viscosities within the range of approximately 1,690–3,800 Pa.s at the nozzle orifice enable successful printing using a 200-micron conical nozzle and an extrusion pressure of 200 kPa. If the viscosity of the ink exceeds this range, it becomes challenging to extrude the ink consistently, leading to intermittent filament formation or potential nozzle clogging. Conversely, if the maximum viscosity of the ink falls below this range, the ink is expelled too rapidly, resulting in collapsed structures with poor shape fidelity.

To extend the predictability of whether the ink is printable under more generalizable printing conditions, we propose an empirically-defined non-dimensional Printability number (Pr), which accounts for extrusion pressure, viscous, inertial, and geometric factors, as expressed in Eq. 12:

$$Pr = \frac{\eta.\dot{\gamma}}{P}\frac{V_N}{V_f}\frac{D_N}{\delta} \tag{12}$$

where P (Pa) is the printing pressure, η (Pa.sec) is the nozzle maximum viscosity, $\dot{\gamma}$ (sec^{-1}) is the nozzle maximum shear rate, V_f (m/sec) is the nozzle peak fluid velocity of the ink, V_N (m/sec) is the nozzle raster speed, D_N (m) is the nozzle diameter, and δ (m) is the distance between the nozzle tip and the printing plane (as depicted schematically in Figure 7A). Upon tabulation of the computationally

TABLE 1 Consistency coefficient (K) and the flow behavior index (n) of different HA:PCL suspensions.

PCL% (%)	HA:PCL Ratio	log(K) mean ± SD	n mean ± SD
15	3:1	2.047 ± 0.003	0.969 ± 0.079
15	6:1	2.102 ± 0.041	0.706 ± 0.007
15	7:1	3.031 ± 0.122	0.714 ± 0.018
15	8:1	3.153 ± 0.043	0.710 ± 0.017
15	9:1	3.125 ± 0.109	0.803 ± 0.037
20	3:1	2.326 ± 0.091	0.784 ± 0.042
20	6:1	2.705 ± 0.045	0.620 ± 0.008
20	7:1	3.323 ± 0.080	0.787 ± 0.068
20	8:1	3.500 ± 0.100	0.768 ± 0.057
25	1:1	2.615 ± 0.048	0.809 ± 0.047
25	3:1	3.084 ± 0.059	0.772 ± 0.019
25	6:1	3.164 ± 0.121	0.755 ± 0.028
25	7:1	3.256 ± 0.033	0.742 ± 0.045
30	1:1	2.644 ± 0.064	0.926 ± 0.038
30	3:1	3.255 ± 0.082	0.707 ± 0.004
30	6:1	3.345 ± 0.110	0.698 ± 0.033

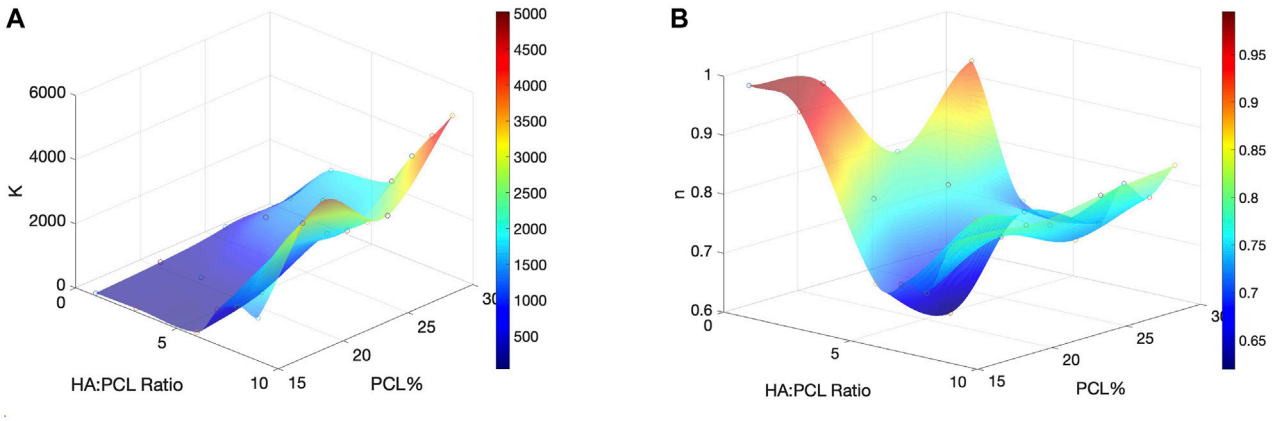

FIGURE 4
Effects of polymer % and microparticle weight ratio on flowability and shear thinning of the HA:PCL inks. **(A)** The consistency coefficient (K), the ink's resistance to flow under shear stress, as a function of PCL% and HA:PCL ratio. **(B)** The flow behavior index (*n*), which determines the relationship between shear stress (τ) and shear rate (γ) in the ink as a function of PCL% and HA:PCL ratio.

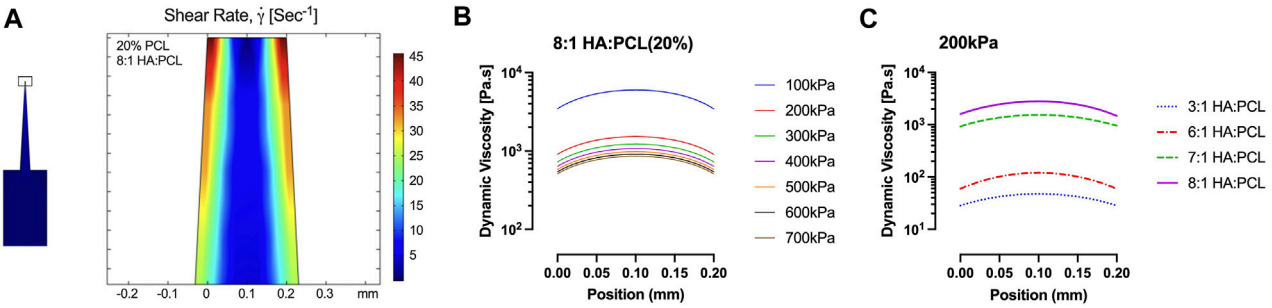

FIGURE 5
COMSOL® simulation of HA:PCL ink flow inside a 200-micron 3D printing conical nozzle. **(A)** The computed distribution profile of the shear rate within the nozzle of an ink consisting of 20% PCL with 8:1 HA:PCL ratio. **(B)** The dynamic viscosity profiles at the ejection orifice with varying extrusion pressures from 100 kPa to 700 kPa, representing the operating range of the BioX™ bioprinter. **(C)** The dynamic viscosity profiles at the ejection orifice of the nozzle for a 20% PCL ink with various HA:PCL ratios under a 200 kPa extrusion pressure were used in the qualitative assessment of printability.

calculated *Pr* and mapping to qualitative printability assessments, we determined that the range of 20 < *Pr* < 30 reliably predicted the printable ink formulations (Figure 7B). Inks with *Pr* < 20 generally indicate soft materials that do not maintain 3D printed form, and *Pr* > 30 is generally hard to print or unprintable.

3.4 HA:PCL inks exhibit hyperelastic mechanical properties

To evaluate the mechanical properties of the 3D printed scaffolds generated using several printable ink formulations, compression testing of 3D printed cylindrical disks were performed. All tested ink formulations exhibited hyperelastic stress-strain behaviors, in which three distinct regions or behaviors could be observed, an initial elastic region (up to ~0.1 strain), a hyperelastic region (up to ~0.6 strain), and a plastic region at strains >0.6 (Figure 8A). To quantify this mechanical behavior, the toughness of the scaffolds, defined as the area under the stress-strain curve up to 0.6 strain, was calculated. The toughness of the scaffolds decreased significantly with increased HA:PCL ratio, which is concomitant with decreased PCL% (Figure 8B). The moduli of the initial elastic, hyperelastic, and plastic regions were also calculated (Figures 8C–E). The initial elastic modulus decreased significantly with decreased PCL% despite these formulations' increased HA:PCL ratio (Figure 8C). The hyperelastic modulus was significantly lower than the initial elastic modulus regardless of the HA:PCL ratio or PCL% and tended to increase with increased HA:PCL ratio (Figure 8D). The plastic modulus was significantly higher than the initial elastic and the hyperelastic moduli but did not significantly vary with the HA:PCL ratio or PCL% (Figure 8E).

Furthermore, the stress-strain curves were fitted to a five-parameter Mooney-Rivlin constitutive model, which successfully described the hyperelastic behavior of the HA:PCL scaffolds under compression (Figure 9A). Quantification of the model parameter C1, which represents the linear response of the material to the first invariant of the deformation tensor, demonstrated that the

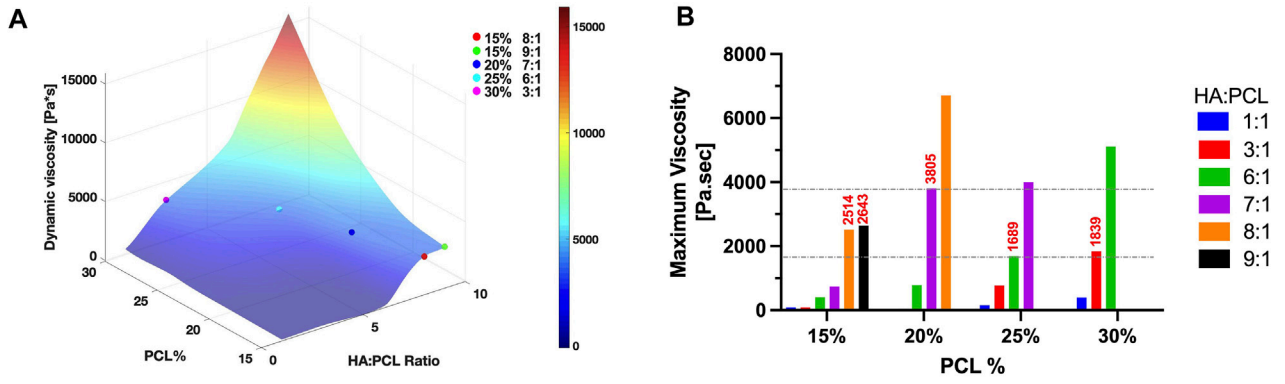

FIGURE 6
Optimization of dynamic viscosity range for enhanced HA:PCL ink printability. **(A)** Surface plot of computed maximum viscosities at nozzle ejection orifice for all simulated inks at an extrusion pressure of 200 kPa. The plot illustrates clusters of printable formulations (represented by circles) where viscosities closely align within a defined range. **(B)** Computed maximum viscosities at the nozzle's orifice for all inks tested experimentally. Viscosities ranging from 1,690 to 3,800 Pa.s at the nozzle orifice enable successful printing using a 200-micron conical nozzle and an extrusion pressure of 200 kPa.

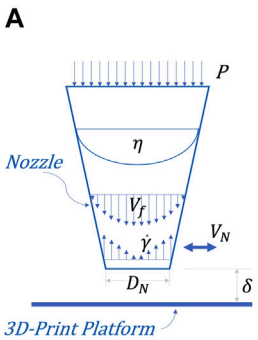

B

PCL Wt %	HA:PCL Ratio	*Pr*
15%	1:1	0.80
15%	3:1	0.95
15%	6:1	4.58
15%	7:1	8.31
15%	**8:1**	**28.30**
15%	**9:1**	**27.41**
20%	1:1	1.57
20%	3:1	1.42
20%	6:1	9.65
20%	**7:1**	**26.30**
20%	8:1	46.53
20%	9:1	59.56
25%	1:1	3.35
25%	3:1	13.30
25%	**6:1**	**21.69**
25%	7:1	34.51
25%	8:1	40.88
30%	1:1	3.84
30%	**3:1**	**25.47**
30%	6:1	58.22

FIGURE 7
Printability assessment of HA:PCL inks based on the empirically-defined non-dimensional Printability Number (Pr). **(A)** Schematic representation of the parameters involved in the calculation of the Printability number (Pr), including P (printing pressure), η (nozzle maximum viscosity), $\dot{\gamma}$ (nozzle maximum shear rate), V_f (nozzle peak fluid velocity), V_N (nozzle raster speed), D_N (nozzle diameter), and δ (distance between the nozzle tip and the printing plane). **(B)** The relationship between the calculated Pr values and qualitative printability assessments. HA:PCL inks within the range of $20 < Pr < 30$ are predicted to be printable, maintaining their 3D printed form (green shades). HA:PCL inks with $Pr < 20$ generally exhibit soft materials that do not hold their printed structure (grey shades), while $Pr > 30$ indicates materials that are difficult or unprintable (red shades).

material's resistance to volumetric changes (compression) decreases with decreased PCL% despite the increased HA:PCL ratio (Figure 9B). Similarly, C2, which characterizes the nonlinear response of the material to the second invariant of the deformation tensor, reflected that the material's resistance to distortional deformations (shear) also decreased with decreased PCL% despite the increased HA:PCL ratio (Figure 9C). Parameters C3, C4, and C5 represent higher-order non-linear behaviors of the deformation tensor, and their negative values are likely explained by inverse coupling between compressive and shear deformations and complex anisotropic phenomena (Table 2) (Lashkari and Mahboubi, 2015).

4 Discussion

The successful application of low-temperature extrusion three-dimensional printing (LTE-3DP) using viscous ceramic-polymer

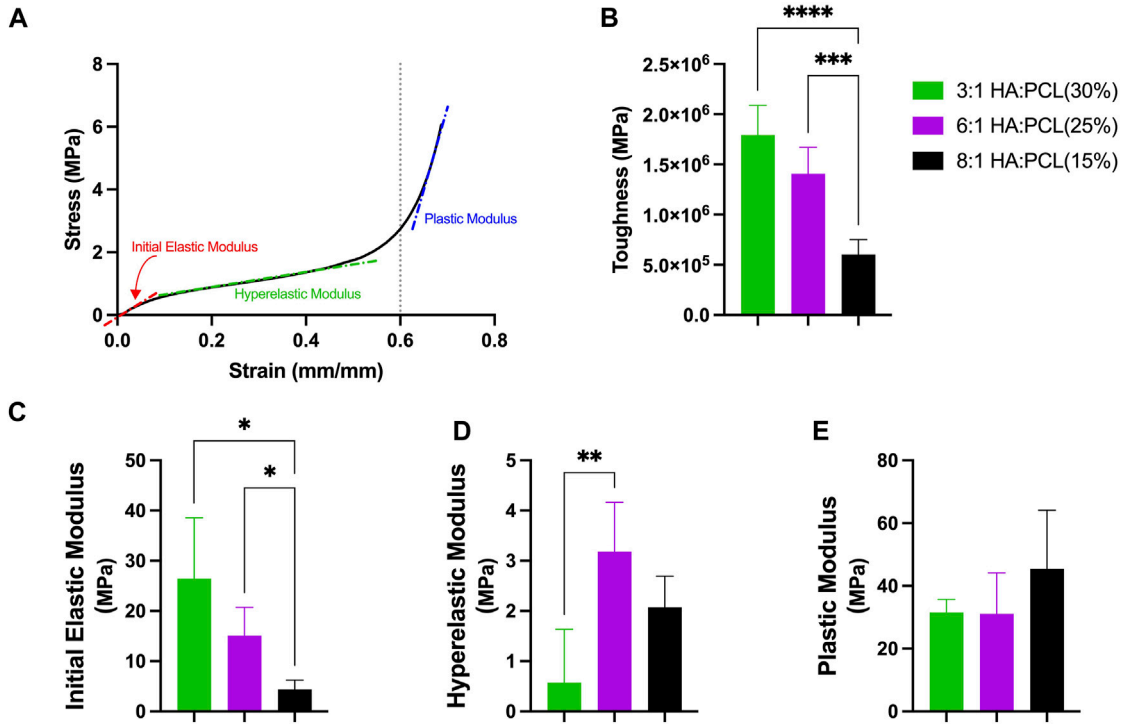

FIGURE 8
Mechanical compressive properties of 3D printed HA:PCL scaffolds. **(A)** Hyperelastic stress-strain curves of the printed cylindrical disks exhibited three distinct regions: initial elastic, hyperelastic, and plastic regions. **(B)** The toughness of the scaffolds, measured as the area under the stress-strain curve up to 0.6 strain, decreased with decreased PCL% despite the increased HA:PCL ratio. **(C)** The initial elastic modulus decreased significantly with reduced PCL% despite the increased HA:PCL ratio. **(D)** The hyperelastic modulus was significantly lower than the initial elastic modulus and tended to increase with increased HA:PCL ratio even as the PCL% decreased. **(E)** The plastic modulus was significantly higher than the initial elastic and hyperelastic moduli and did not significantly vary with the HA:PCL ratio or PCL%. Data presented as mean ± Standard deviation (n = 6). Asterisks indicate significant differences using one-way ANOVA and Bonferroni-corrected multiple comparisons.

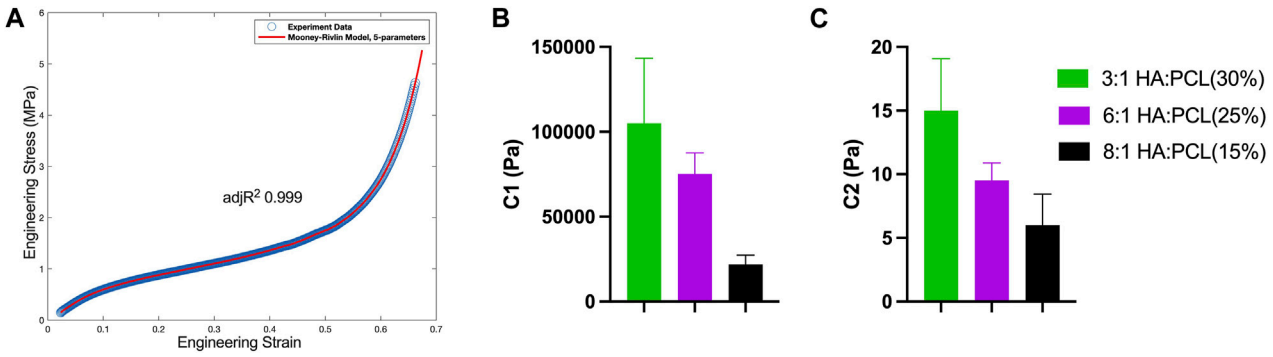

FIGURE 9
Characterization of the hyperelastic behavior and material parameters of HA:PCL scaffolds. **(A)** A five-parameter Mooney-Rivlin constitutive model was fitted to the experimental compressive stress-strain curves of 3D printed HA:PCL scaffolds. **(B)** Parameter C1 reveals a decrease in the material's resistance to volumetric changes (compression) with increased HA:PCL ratio. **(C)** Parameter C2 indicates a decrease in the material's resistance to distortional deformations (shear) with increased HA:PCL ratio.

inks for bone tissue engineering has been demonstrated in various studies (Leukers et al., 2005; Seitz et al., 2005; Jakus et al., 2016a; Roohani-Esfahani et al., 2016; Trombetta et al., 2017; Wang et al., 2017; Du et al., 2018; Huang et al., 2019; Zhang et al., 2019). However, the optimal implementation of LTE-3DP for a specific ink relies on several variables. These variables encompass the polymer's type, molecular weight, concentration, the polymer solvent and additives like plasticizers or surfactants, as well as the characteristics of the ceramic particles, such as type, size, and weight ratio of the ceramic-polymer suspension. Notably, these variables

TABLE 2 Mooney-Rivlin constitutive model parameters of 3D printed HA:PCL scaffolds.

	3:1 HA:PCL (30%)	6:1 HA:PCL (25%)	8:1 HA:PCL (15%)
C1	105,000 ± 93,700	75,200 ± 30,200	21,793 ± 13,402
C2	15.00 ± 10.00	9.51 ± 4.40	6.00 ± 6.00
C3	−782 ± 523	−568 ± 188	−335 ± 276
C4	−14,600 ± 37,300	−28,800 ± 37,200	−24,067 ± 36,205
C5	−9,290 ± 16,600	−3,480 ± 9,490	2,780 ± 5,492

influence the ink's viscosity and flow behavior during the printing process and not only influence the printability but also affect the scaffold stability and shape fidelity as well as the mechanical properties of the resulting 3D printed scaffolds. Despite the recognition of the importance of these variables (Gillispie et al., 2020; Naghieh and Chen, 2021; Tarassoli et al., 2021), few studies have attempted to experimentally establish how these ink variables could influence the printability (M'Barki et al., 2017; Paul D L et al., 2023).

Printability has been defined as "the capability to form and maintain reproducible 3D scaffolds from ink using the bioprinting technique" (Naghieh and Chen, 2021). This definition implies that a printable ink must allow its extrusion as continuous filaments matching the size of the extrusion nozzle and then sustain size and shape fidelity as the printed scaffold hardens. In this study, we systematically varied the composition of HA:PCL inks, a ceramic-polymer mixture frequently used in bone tissue engineering studies, and assessed their rheological properties to determine their shear thinning (dynamic viscosity at varying shear rates) and solid-like behavior (storage modulus). By systematically altering the PCL weight percentage and the HA:PCL weight ratio, we demonstrated that while HA:PCL inks predictably behave as viscous non-Newtonian fluids at higher weight percentage and HA:PCL ratio, they exhibited significant shear thinning at higher shear rates that could enhance their extrusion through a 3D printing nozzle. We qualitatively identified the printable ink compositions based on the printability definition by Naghieh and Chen (2021). Finally, we simulated the flow of the ink through a standard conical nozzle geometry and extrusion pressure matching the BioX™ bioprinter using an incompressible, non-Newtonian [Herschel-Bulkley-Papanastasiou (HBP)] constitutive model and the experimentally measured rheological behaviors. This simulation allowed us to identify the range of printable viscosities and shear rates within the extrusion for each printable ink formulation. With this information, we defined a novel non-dimensional Printability (*Pr*) number that considers the ink's rheological behavior and the bioprinter-specific factor to predict whether an ink can be extruded as continuous filaments that sustain the form and shape fidelity upon printing. While the *Pr* number was derived for PCL inks containing ≤30 micron-sized HA microparticles, a specific nozzle geometry, and a fixed extrusion pressure of 200 kPa, it remains to be determined if it can be generalizable. Regardless, the approach represents a framework to predict the printability of ceramic-polymer ink formulations, which could help streamline the 3D printing of novel inks for bone tissue engineering.

A recent study investigated the properties of ceramic inks made from tri-calcium phosphate (TCP):Pluronic surfactant for extrusion-based printing [direct ink writing (DIW)]. The study analyzed the viscosity, shear rate, and viscoelastic behavior of the inks, examined the impact of TCP concentration, dispersant content, and binder type on ink rheology, and concluded that the rheological properties of the TCP inks dictate successful printing of high-quality, consistent filaments (Paul D L et al., 2023). A similar approach was proposed by M'Barki and co-authors, which explored the time-dependent gelation and rheological behaviors required for successful direct ink writing (DIW) of dense and strong ceramic objects using boehmite (a crystalline form of aluminum oxide) gels as ink (M'Barki et al., 2017). They similarly proposed a dimensionless criterion, based on rheological properties, that emphasizes the importance of considering capillary forces and gravitational slumping in determining the printability and shape fidelity of printed objects, which can then be sintered to produce dense ceramics with flexural strengths rivaling bioinert alumina produced using conventional methods. These studies and ours provide important insights for designing inks tailored for printing dense materials based on their rheological properties.

We also demonstrated the hyperelastic mechanical properties of the HA:PCL 3D printed ink, which corroborates findings by others (Jakus et al., 2016a). These scaffolds generally exhibited stress-strain behaviors that featured two inflection points and three defined regions, which could be fitted using a five-parameter Mooney-Rivlin constitutive model (Kumar and Rao, 2016). In the initial elastic region, the HA-PCL mixture elastic behavior is primarily attributed to the polymer matrix, which provides flexibility and resilience. As the stress increases beyond the elastic limit of the initial region, the material transitions into a hyperelastic region. This behavior arises from the interaction between the polymer matrix and the ceramic micro-particles. The polymer matrix may undergo deformation and reorientation of polymer chains, contributing to the hyperelastic behavior. The ceramic micro-particles may also undergo redistribution and densification, leading to increased compressive modulus with an increased HA weight ratio (Birman et al., 2013). As the applied deformation increases, the PCL polymer enters a higher-strain region where it undergoes plastic deformation, corresponding to the third region. The molecular chains start to unravel, slip, and reorient, resulting in a permanent change in shape even after stress removal. This behavior is characteristic of the polymer's ability to sustain large strains without undergoing structural failure. Further, the plastic modulus of the mixture depends on the weight ratio of the ceramic microparticles and the polymer, as well as the distribution and densification of the particles within the matrix. As observed experimentally, a higher volume fraction and densification of the ceramic particles can lead to a higher plastic modulus Field (Islam et al., 2018). Overall, our results demonstrated that the initial elastic compressive moduli and the toughness of the scaffolds decrease with reduced PCL% despite the increased HA:PCL ratio in printable inks. The decreased mechanical properties were probably due to decreased PCL% and not the increased HA weight ratio in these printable inks. Therefore, determining the PCL% and weight ratio of HA in the PCL polymer must consider the target mechanical properties. In our experience, printable inks with higher HA weight ratios were achievable only when we reduced PCL% in the solvent, which resulted in more compliant scaffolds under low deformations. The compromise in mechanical properties must be balanced against the osteoinductive benefits of high HA ratios when these 3D-printed scaffolds are used as bone void fillers.

5 Conclusion

In conclusion, this study focused on optimizing low-temperature extrusion three-dimensional printing (LTE-3DP) of hydroxyapatite-polycaprolactone mixture inks. We investigated the influence of various variables, including the polymer type, concentration, solvent, additives, and ceramic particle characteristics, on the printability, shape fidelity, and mechanical properties of the 3D-printed scaffolds. By systematically varying the composition of HA: PCL inks, we demonstrated their non-Newtonian flow behavior and identified printable ink formulations based on their rheological properties. We also developed a novel non-dimensional Printability (Pr) number to predict the extrudability and shape fidelity of the inks. Additionally, we examined the hyperelastic mechanical properties of the HA:PCL scaffolds and observed a complex stress-strain response attributed to the interactions between the polymer matrix and ceramic micro-particles. The weight ratio of HA in the PCL polymer was found to impact the compressive moduli and toughness of the scaffolds. These findings contribute to understanding the influence of ink variables on LTE-3DP and provide insights for designing inks with tailored rheological and mechanical properties for bone tissue engineering applications. Future research should validate and extend these findings to other ceramic-polymer ink systems and explore their applicability in the broader field of 3D printing for bone tissue engineering.

Data availability statement

The raw data supporting the conclusion of this article will be made available by the authors, without undue reservation.

Author contributions

Conceptualization, MY and HA; methodology, MY; data acquisition, MY; numerical simulations, MY; writing–original draft preparation, MY; writing–review and editing, HA; supervision, HA; project administration, HA; funding acquisition, HA. All authors contributed to the article and approved the submitted version.

Funding

This study was supported by NIAMS/NIH grants P50AR072000 and P30AR069655. The content is solely the responsibility of the authors and does not necessarily represent the official views of the National Science Foundation, National Institutes of Health.

Conflict of interest

The authors declare that the research was conducted in the absence of any commercial or financial relationships that could be construed as a potential conflict of interest.

Publisher's note

References

Athanasiou, V. T., Papachristou, D. J., Panagopoulos, A., Saridis, A., Scopa, C. D., and Megas, P. (2009). Histological comparison of autograft, allograft-DBM, xenograft, and synthetic grafts in a trabecular bone defect: an experimental study in rabbits. *Med. Sci. Monit.* 16, BR24–BR31.

Birman, V., Chandrashekhara, K., Hopkins, M. S., and Volz, J. S. (2013). Strength analysis of particulate polymers. *Compos. Part B Eng.* 54, 278–288. doi:10.1016/j.compositesb.2013.05.009

Bohner, M. (2010). Design of ceramic-based cements and putties for bone graft substitution. *Eur. Cell Mater* 20, 1–12. doi:10.22203/ecm.v020a01

Campana, V., Milano, G., Pagano, E., Barba, M., Cicione, C., Salonna, G., et al. (2014). Bone substitutes in orthopaedic surgery: from basic science to clinical practice. *J. Mater. Sci. Mater. Med.* 25, 2445–2461. doi:10.1007/s10856-014-5240-2

Chen, G., Dong, C., Yang, L., and Lv, Y. (2015). 3D scaffolds with different stiffness but the same microstructure for bone tissue engineering. *ACS Appl. Mater. interfaces* 7, 15790–15802. doi:10.1021/acsami.5b02662

Dorozhkin, S. V. (2010). Bioceramics of calcium orthophosphates. *Biomaterials* 31, 1465–1485. doi:10.1016/j.biomaterials.2009.11.050

Du, X., Fu, S., and Zhu, Y. (2018). 3D printing of ceramic-based scaffolds for bone tissue engineering: an overview. *J. Mater. Chem. B* 6, 4397–4412. doi:10.1039/c8tb00677f

Dwivedi, R., Kumar, S., Pandey, R., Mahajan, A., Nandana, D., Katti, D. S., et al. (2020). Polycaprolactone as biomaterial for bone scaffolds: review of literature. *J. Oral Biol. Craniofacial Res.* 10, 381–388. doi:10.1016/j.jobcr.2019.10.003

Frigaard, I. A., and Nouar, C. (2005). On the usage of viscosity regularisation methods for visco-plastic fluid flow computation. *J. Newt. Fluid Mech.* 127, 1–26. doi:10.1016/j.jnnfm.2005.01.003

Gillispie, G., Prim, P., Copus, J., Fisher, J., Mikos, A. G., Yoo, J. J., et al. (2020). Assessment methodologies for extrusion-based bioink printability. *Biofabrication* 12, 022003. doi:10.1088/1758-5090/ab6f0d

Hak, D. J., Fitzpatrick, D., Bishop, J. A., Marsh, J. L., Tilp, S., Schnettler, R., et al. (2014). Delayed union and nonunions: epidemiology, clinical issues, and financial aspects. *Injury* 45, S3–S7. doi:10.1016/j.injury.2014.04.002

Huang, Y.-H., Jakus, A. E., Jordan, S. W., Dumanian, Z., Parker, K., Zhao, L., et al. (2019). Three-dimensionally printed hyperelastic bone scaffolds accelerate bone regeneration in critical-size calvarial bone defects. *Plastic Reconstr. Surg.* 143, 1397–1407. doi:10.1097/prs.0000000000005530

Islam, M. R., Tudryn, G., Bucinell, R., Schadler, L., and Picu, R. C. (2018). Mechanical behavior of mycelium-based particulate composites. *J. Mater. Sci.* 53, 16371–16382. doi:10.1007/s10853-018-2797-z

Jakus, A. E., Koube, K. D., Yoo, S. C., Rutz, A. L., Jordan, S. W., Galiano, R. D., et al. (2016a). Hyperelastic bone: A highly versatile, growth factor-free, osteoregenerative, scalable, and surgically friendly biomaterial. *Sci. Transl. Med.* 8, 358ra127. doi:10.1126/scitranslmed.aaf7704

Jakus, A. E., Rutz, A. L., and Shah, R. N. (2016b). Advancing the field of 3D biomaterial printing. *Biomed. Mater.* 11, 014102. doi:10.1088/1748-6041/11/1/014102

Kumar, N., and Rao, V. V. (2016). Hyperelastic mooney-rivlin model: determination and physical interpretation of material constants. *MIT Int. J. Mech. Eng.* 6, 43–46.

Lashkari, A., and Mahboubi, M. (2015). Use of hyper-elasticity in anisotropic clay plasticity models. *Sci. Iran.* 22, 1643–1660.

Leukers, B., Glkan, H., Irsen, S. H., Milz, S., Tille, C., Schieker, M., et al. (2005). Hydroxyapatite scaffolds for bone tissue engineering made by 3D printing. *J. Mater. Sci. Mater. Med.* 16, 1121–1124. doi:10.1007/s10856-005-4716-5

M'barki, A., Bocquet, L., and Stevenson, A. (2017). Linking rheology and printability for dense and strong ceramics by direct ink writing. *Sci. Rep.* 7, 6017. doi:10.1038/s41598-017-06115-0

Miranda, M. A., and Moon, M. S. (2007). Treatment strategy for nonunions and malunions. *Surg. Treat. Orthop. trauma* 1, 77–100.

Mouriño, V., and Boccaccini, A. R. (2010). Bone tissue engineering therapeutics: controlled drug delivery in three-dimensional scaffolds. *J. R. Soc. Interface* 7, 209–227. doi:10.1098/rsif.2009.0379

Naghieh, S., and Chen, X. (2021). Printability–A key issue in extrusion-based bioprinting. *J. Pharm. Analysis* 11, 564–579. doi:10.1016/j.jpha.2021.02.001

Paul, D. L, B., Praveen, A. S., Čepová, L., and Elangovan, M. (2023). Rheological behavior and printability study of tri-calcium phosphate ceramic inks for direct ink writing method. *Polymers* 15, 1433. doi:10.3390/polym15061433

Roohani-Esfahani, S.-I., Newman, P., and Zreiqat, H. (2016). Design and fabrication of 3D printed scaffolds with a mechanical strength comparable to cortical bone to repair large bone defects. *Sci. Rep.* 6, 19468. doi:10.1038/srep19468

Seitz, H., Rieder, W., Irsen, S., Leukers, B., and Tille, C. (2005). Three-dimensional printing of porous ceramic scaffolds for bone tissue engineering. *J. Biomed. Mater. Res. Part B Appl. Biomaterials Official J. Soc. Biomat* 74, 782–788. doi:10.1002/jbm.b.30291

Shi-Ju, E., Chen, Y.-K., Cao, J.-B., Li, J.-L., Gao, Z., Luo, H.-P., et al. (2020). Determination method of constitutive model parameters of dielectric elastomer material. *AIP Adv.* 10. doi:10.1063/1.5124334

Shor, L., Geri, S., Wen, X., Gandhi, M., and Sun, W. (2007). Fabrication of three-dimensional polycaprolactone/hydroxyapatite tissue scaffolds and osteoblast-scaffold interactions *in vitro*. *Biomaterials* 28, 5291–5297. doi:10.1016/j.biomaterials.2007.08.018

Tarassoli, S. P., Jessop, Z. M., Jovic, T., Hawkins, K., and Whitaker, I. S. (2021). Candidate bioinks for extrusion 3D bioprinting-A systematic review of the literature. *Front. Bioeng. Biotechnol.* 9, 616753. doi:10.3389/fbioe.2021.616753

Travitzky, N., Bonet, A., Dermeik, B., Fey, T., Filbert-Demut, I., Schlier, L., et al. (2014). Additive manufacturing of ceramic-based materials. *Adv. Eng. Mater.* 16, 729–754. doi:10.1002/adem.201400097

Trombetta, R., Inzana, J. A., Schwarz, E. M., Kates, S. L., and Awad, H. A. (2017). 3D printing of calcium phosphate ceramics for bone tissue engineering and drug delivery. *Ann. Biomed. Eng.* 45, 23–44. doi:10.1007/s10439-016-1678-3

Umale, S., Deck, C., Bourdet, N., Dhumane, P., Soler, L., Marescaux, J., et al. (2013). Experimental mechanical characterization of abdominal organs: liver, kidney & spleen. *J. Mech. Behav. Biomed. Mater.* 17, 22–33. doi:10.1016/j.jmbbm.2012.07.010

Von Boetticher, A., Turowski, J. M., Mcardell, B. W., Rickenmann, D., and Kirchner, J. W. (2016). DebrisInterMixing-2.3: a finite volume solver for three-dimensional debris-flow simulations with two calibration parameters-Part 1: model description. *Geosci. Model Dev.* 9, 2909–2923. doi:10.5194/gmd-9-2909-2016

Wang, W., and Yeung, K. W. K. (2017). Bone grafts and biomaterials substitutes for bone defect repair: A review. *Bioact. Mater.* 2, 224–247. doi:10.1016/j.bioactmat.2017.05.007

Wang, C., Zhao, Q., and Wang, M. (2017). Cryogenic 3D printing for producing hierarchical porous and rhBMP-2-loaded Ca-P/PLLA nanocomposite scaffolds for bone tissue engineering. *Biofabrication* 9, 025031. doi:10.1088/1758-5090/aa71c9

Wang, Z., Guo, W., Ding, W., Liu, K., Qin, W., Wang, C., et al. (2023). Numerical study on the hydrodynamic properties of bentonite slurries with Herschel-Bulkley-Papanastasiou rheology model. *Powder Technol.* 419, 118375. doi:10.1016/j.powtec.2023.118375

Zhang, J., Liu, W., Schnitzler, V., Tancret, F., and Bouler, J.-M. (2014). Calcium phosphate cements for bone substitution: chemistry, handling and mechanical properties. *Acta Biomater.* 10, 1035–1049. doi:10.1016/j.actbio.2013.11.001

Zhang, L., Yang, G., Johnson, B. N., and Jia, X. (2019). Three-dimensional (3D) printed scaffold and material selection for bone repair. *Acta Biomater.* 84, 16–33. doi:10.1016/j.actbio.2018.11.039